

On the generation and destruction mechanisms of arch vortices in urban fluid flows





Cite as: Phys. Fluids **34**, 051702 (2022); <https://doi.org/10.1063/5.0088305>

Submitted: 15 February 2022 • Accepted: 08 April 2022 • Published Online: 03 May 2022

Eneko Lazpita,  Álvaro Martínez-Sánchez,  Adrián Corrochano, et al.

COLLECTIONS

 This paper was selected as Featured

 This paper was selected as Scilight



View Online



Export Citation



CrossMark

ARTICLES YOU MAY BE INTERESTED IN

[Perimeter leakage of face masks and its effect on the mask's efficacy](#)

Physics of Fluids **34**, 051902 (2022); <https://doi.org/10.1063/5.0086320>

[Understanding urban fluid flows urgent for dispersing pollution](#)

Scilight **2022**, 181101 (2022); <https://doi.org/10.1063/10.0010423>

[On Oreology, the fracture and flow of “milk's favorite cookie”[®]](#)

Physics of Fluids **34**, 043107 (2022); <https://doi.org/10.1063/5.0085362>

APL Machine Learning

Open, quality research for the networking communities

MEET OUR NEW EDITOR-IN-CHIEF

LEARN MORE



On the generation and destruction mechanisms of arch vortices in urban fluid flows



Cite as: Phys. Fluids **34**, 051702 (2022); doi: [10.1063/5.0088305](https://doi.org/10.1063/5.0088305)

Submitted: 15 February 2022 · Accepted: 8 April 2022 ·

Published Online: 3 May 2022



View Online



Export Citation



CrossMark

Eneko Lazpita,¹ Álvaro Martínez-Sánchez,² Adrián Corrochano,¹ Sergio Hoyas,² Soledad Le Clainche,¹ and Ricardo Vinuesa^{3,a)}

AFFILIATIONS

¹School of Aerospace Engineering, Universidad Politécnica de Madrid, Madrid E-28040, Spain

²Instituto de Matemática Pura y Aplicada, Universitat Politècnica de València, Camino de Vera, 46024 València, Spain

³FLOW, Engineering Mechanics, KTH Royal Institute of Technology, SE-100 44 Stockholm, Sweden

^{a)} Author to whom correspondence should be addressed: rvinuesa@mech.kth.se

ABSTRACT

This study uses higher-order dynamic mode decomposition to analyze a high-fidelity database of the turbulent flow in an urban environment consisting of two buildings separated by a certain distance. We recognize the characteristics of the well-known arch vortex forming on the leeward side of the first building and document this vortex's generation and destruction mechanisms based on the resulting temporal modes. We show that the arch vortex plays a prominent role in the dispersion of pollutants in urban environments, where its generation leads to an increase in their concentration; therefore, the reported mechanisms are of extreme importance for urban sustainability.

Published under an exclusive license by AIP Publishing. <https://doi.org/10.1063/5.0088305>

Urban areas are essential in today's society, with 70% of the world's population expected to live in cities by 2050.¹ Cities contribute more than 60% of the total greenhouse gas emissions and are, therefore, essential players in the fight against climate change.² Furthermore, sustainable cities is the eleventh Sustainable Development Goal of the United Nations. Some attempts have been made to implement predictive models and study the physics associated with the turbulent fluid flows in urban areas.³ In particular, we want to identify coherent flow features by applying modal decomposition to turbulent urban flows. This would allow for a better design of buildings and cities.

The arch vortex (which can be observed in Fig. 1) is a vortical structure that appears on the leeward side of a wall-mounted obstacle. It consists of two legs and one roof. In the latter, the flow rotates in the wall-normal direction. In the former, it rotates in the spanwise direction. This vortex has been experimentally studied by Becker *et al.*⁴ for different angles of incidence (AOI). The wake of the flow around a single obstacle was studied by Kawai *et al.*⁵ using conditional sampling with stereoscopic particle-image velocimetry (SPIV). They obtained an image of the temporal evolution of the arch vortex, which exhibits characteristics similar to those of a Kármán vortex street. However, the boundary layer used in their study might not have been fully representative of an atmospheric boundary layer (ABL). The coherent structures obtained behind two aligned cubic obstacles were studied by Martinuzzi and Havel⁶ for several distances between the obstacles.

AbuOmar and Martinuzzi^{7,8} studied pyramid-shaped obstacles. Simplified urban environments with matrices of obstacles and different angles of incidence (AOI) were studied by Monnier *et al.*⁹ Other studies have analyzed the flow around obstacles using high-fidelity numerical simulations.¹⁰

Another relevant vortical structure is the horseshoe vortex, which is formed on the windward side of the obstacle. It is responsible (together with the vortex-flow pattern) for the flow distribution around an obstacle. The cross-sectional shape of the obstacle has a high influence on the presence and formation of the horseshoe vortex, as discussed by Sumer *et al.*¹¹ Although both the arch and the horseshoe vortices have been studied in other works mentioned previously, there are several open questions regarding the mechanisms that create and break these structures. In this study, we address this critical aspect by analyzing the data from a high-resolution simulation of a urban flow by means of various modal-decomposition algorithms.

The simulation and modal-decomposition methods have been explained in another article by the same authors.¹² The velocity field is given by $\mathbf{v}(x, y, z, t)$, where x , y , and z are the streamwise, wall-normal, and spanwise directions, respectively, and t is time. Every velocity is normalized with the free stream velocity. The components of the velocity are $\mathbf{v} = (u, v, w)$, which denote, respectively, the streamwise, wall-normal, and spanwise components. Using Reynolds decomposition, is defined as $\mathbf{v} = \mathbf{V} + \tilde{\mathbf{v}}$, where $\mathbf{V} = \bar{\mathbf{v}}$ is the average

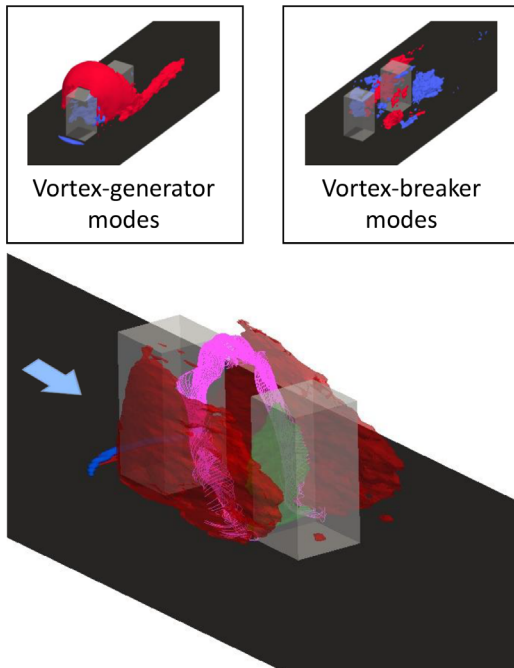


FIG. 1. Classification of the different modes obtained with HODMD. Bottom panel: blue, $v' = 0.7$; red, $u' = 0.6$; and green, $w' = 0.8$. Mean streamlines representing the arch vortex are plotted in magenta, while the two obstacles are in transparent gray. Top panels: streamwise velocity of the modes normalized using the L_∞ -norm. The iso-values employed are given by $a U_{\max}$ (red) and $b U_{\min}$ (blue). Top-left: vortex-generator modes with $a = 0.8$ and $b = 0.5$. Top-right: vortex-breaker modes with $a = 0.3$ and $b = 0.45$. All cases corresponds to the SF case (see definition below). The arrow indicates the flow direction.

in time and \tilde{v} is the turbulent fluctuation. Primes are reserved for intensities $v' = \overline{v^2}^{1/2}$.

Briefly, we have simulated the turbulent flow in a simplified urban environment consisting of two obstacles, where different regimes are observed when varying the separation between them.¹³ According to the classification by Oke,¹⁴ the first regime is the so-called skimming-flow (SF) configuration, in which the distance between the buildings is the lowest; hence, the second building hinders the development of the wake of the first one. The second case is denoted as the wake-interference (WI) regime, and in this configuration, the effect of the second building on the wake of the first one is less pronounced than in the SF case but still significant. The last case is the isolated-roughness (IR) regime, which is characterized by the highest separation between buildings and exhibits two different phenomena: the first building behaves as an isolated obstacle, and the second building essentially does not affect the development of the wake from the first one. We focus on the WI case in this work, as the main structures can be clearly observed.

Two modal-decomposition methods has been used in this work: proper-orthogonal decomposition (POD)¹⁵ and higher-order dynamic-mode decomposition (HODMD).¹⁶ The HODMD decomposes spatiotemporal data $v(x, y, z, t_k)$, collected at time instant t_k (for convenience expressed as v_k), as an expansion of M modes \mathbf{u}_m , which are weighted by an amplitude a_m as follows:

$$v(x, y, z, t_k) \simeq \sum_{m=1}^M a_m \mathbf{u}_m(x, y, z) e^{(\delta_m + i\omega_m)t_k}, \quad (1)$$

for $k = 1, \dots, K$. These modes oscillate in time with frequency ω_m and may grow, decay, or remain neutral in time according to their growth rate δ_m .

The dominant mode (i.e., the one with the highest amplitude) is located between the frequencies $\omega_m = 1$ and $\omega_m = 1.2$, while the rest of the modes are subharmonics and harmonics of it. In addition, another relevant mode is the one with the lowest frequency (with a value of $\omega_m = 0.11$) since it is the first mode to appear in the spectrum and the periodicity of the main physics is led by its frequency.

Based on Fig. 2, we identify two types of modes, which are shown in Fig. 1: the vortex-generator (A) modes and the vortex-breaker (B) modes. The vortex-generator modes, as their name indicates, are the ones that generate the main structures and vortices. Therefore, they are related to the mechanism that could create the arch and horseshoe vortex. The A modes usually appear in the low-frequency area of the spectrum and have lower amplitude than the B modes. Some of those modes are $\omega_m = 0.13$, $\omega_m = 0.26$, or $\omega_m = 0.39$. The vortex-breaker modes are the ones that break the main structures of the flow and create the turbulent wake. Unlike the vortex-generators, the B modes appear at high frequencies, from the eighth harmonic of the lowest frequency onward. Some breaker-modes are characterized by the following frequencies: $\omega_m = 1.05$, $\omega_m = 1.18$, or $\omega_m = 1.31$.

The model assurance criterion (MAC), which is generally used in aeroelasticity to detect flutter,¹⁹ was used to verify this classification of modes in a quantitative way. Given two vectors \mathbf{u}_i and \mathbf{u}_j , MAC gives just the absolute value of the cosine of the angle between them, namely,

$$MAC = \frac{|\langle \mathbf{u}_i, \mathbf{u}_j \rangle|}{\|\mathbf{u}_i\| \|\mathbf{u}_j\|}.$$

The modes with $MAC > 0.8$ are considered with a similar shape. Let us note that $MAC < 1$ since the small scales connected to the

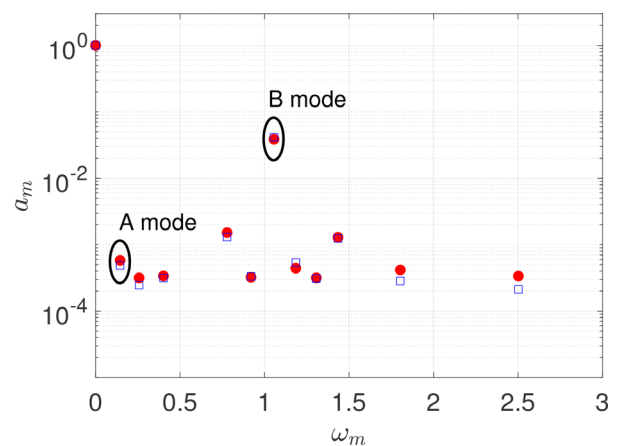


FIG. 2. Spectrum showing the amplitudes vs the frequencies of the temporal modes obtained with HODMD for the WI case with (blue) Euclidean norm and (red) infinity norm. Some A and B modes are highlighted in this figure.

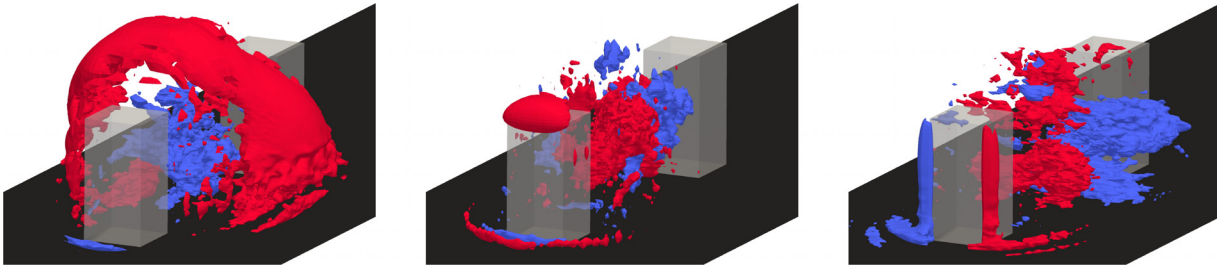


FIG. 3. Isosurfaces of the A mode with $\omega_m = 0.11$. Velocity values of this mode are normalized using the L_∞ -norm. The iso-values employed are given by $a U_{\max}$ (red) and $b U_{\min}$ (blue): left: streamwise velocity with $a = 0.3$ and $b = 0.6$; middle: wall-normal velocity with $a = 0.3$ and $b = 0.4$; and right: spanwise velocity with $a = 0.45$ and $b = 0.45$.

turbulent flow play a dominant role. Hence, the modes calculated will always be different.

It has already been shown in the literature that regions of strong recirculation lead to increased concentration of passive scalars.¹⁷ Then, the A modes, which are related to these potent recirculation areas, could be related to high pollutant concentration.⁹ Similarly, as the B modes are related to breaking the coherent structures present in the turbulent flow, it could be suggested that they are connected with the reduced pollutant concentration. More specifically, the arch vortex is formed by a flow-recirculating area between the two obstacles. This organization suggests that controlling the presence of the A modes may provide insight into strategies to reduce pollution in urban areas. Further research should be carried out to identify A and B modes in databases modeling multi-phase flows, but this remains an open topic for future research.

The mode with the lowest frequency, $\omega_m = 0.11$, has been selected as the most representative A mode. It is connected with the vortex generation mechanism. As shown in Fig. 3, three main large size structures have been identified to construct the distinct vortices: a dome, a cap, and two columns for the streamwise, wall-normal, and spanwise velocities, respectively. The dome is a streamwise structure located just after the first building. It surrounds and interacts with the arch vortex by limiting its expansion and recirculating the flow inside the vortex. The cap-like structure is created on top of the first building, interacting primarily with the roof of the arch vortex. The most representative structure appearing in the spanwise velocity is a column on each side of the first building, affecting the arch vortex legs by creating an ascending rotation of the surrounding flow.

With regard to the influence of the generation mechanisms on the pollutant dispersion, the most unfavorable features may seem to be

the dome and the cap since they could be connected with a delay in the pollutant escape vertically. The columns appearing buildings side in the spanwise direction could have a lower influence. They prevent the flow from extending away from the sides of the buildings but not from escaping from the urban area.

As in the A modes, the dominant vortex-breaker mode, i.e., the one with the highest amplitude of the whole spectrum, is shown in Fig. 4 to assess its main structures. This mode has a frequency of approximately $\omega_m = 1.1$. In this type of mode, three additional structures can be distinguished, one for each velocity component: turbulent wake, coherent cluster between the buildings, and an arrowhead-like shape. The streamwise turbulent wake consists of high-velocity coherent clusters on both sides of the buildings. For the wall-normal direction, the high-velocity clusters appear within the width of the buildings. The arrowhead-like shapes that can be seen in the spanwise direction align with the buildings and are inclined downstream. There is a high recirculation area between the structures with positive and negative fluctuations in the B modes, which is related to the creation of a tunnel-shaped vortical structure between the buildings when breaking the arch vortex.

For the destruction modes, the tendency of the streamwise and wall-normal large-scale structures seems to break the coherent structures by creating clusters that make the flow escape through the sides of the buildings, while the spanwise arrowhead-like structures may help the flow (and the pollutants with it) to escape from the city in a more direct way.

Furthermore, this differentiation between vortex-generating and -breaking modes can be also examined using POD modes, with which those energetically important features can be extracted from the flow. Based on the singular-value decomposition (SVD), the POD method

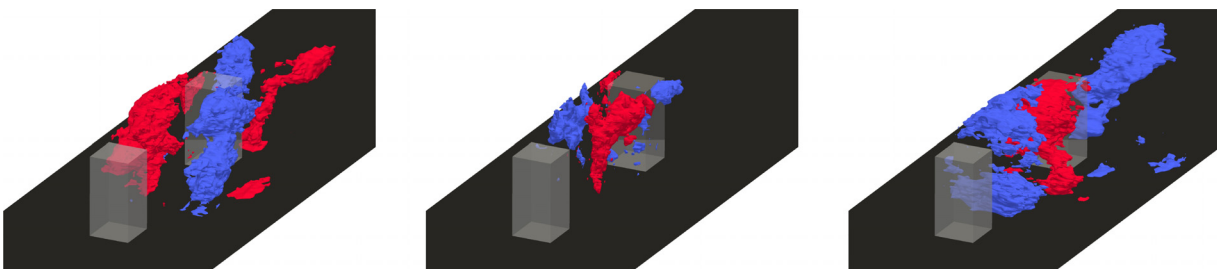


FIG. 4. Isosurfaces of the B mode with $\omega_m = 1.1$. Velocity values of this mode are normalized using the L_∞ -norm. The iso-values employed are given by $a U_{\max}$ (red) and $b U_{\min}$ (blue): left: streamwise velocity with $a = 0.3$ and $b = 0.5$; middle: wall-normal velocity with $a = 0.5$ and $b = 0.4$; and right: spanwise velocity with $a = 0.4$ and $b = 0.5$.

decomposes a set of instantaneous fields or snapshots into a set of spatial and temporal modes and their associated singular values.¹⁵ Here, the aim is to analyze the spatial and temporal modes for the wake-interference regime and state the similarities with the aforementioned modes. The methodology behind POD is based on the correlation matrix, computed in this case with the velocity vector. The method tries to find the directions in the database with the most significant variance, which correspond to the flow structures with the highest kinetic energy in this specific case (since the correlation matrix is formed by the velocity vector). However, these POD modes are not directly related to the energy cascade. The POD modes are orthogonal, and each one is composed of several frequencies, so each POD mode contains information of the flow related to several energy levels of the turbulent energy cascade. Further details on the POD technique and its results are provided in Ref. 12.

In Fig. 5, the spatial modes for the streamwise and spanwise velocity fields are depicted. In addition, an analysis of the temporal coefficients associated with these modes is performed in the frequency domain through the fast Fourier transform (FFT)¹⁸ method. This modal-decomposition technique allows us to classify the time coefficients associated with each spatial mode to low- and high-frequency phenomena, the features of which are very relevant to the vortex-generating and -breaking processes, respectively. Indeed, the first two modes, with an associated frequency matching that of the HODMD B modes ($\omega_m = 1$), are characterized by high-velocity streamwise fluctuations on both sides of the building, which are complemented by spanwise velocity fluctuations aligned with the obstacles. The interaction of these two types of structures results in a tunnel-shaped structure, which suggests that is responsible for the breaking process of the main time-averaged flow structures.¹² Therefore, the vortex-breaking process has been identified as the most energetically relevant mode present in the flow field.

The vortex-generating modes, i.e., the A modes, are related to the third and fourth POD modes, due to their low-frequency behavior ($\omega_m = 0.16$ and $\omega_m = 0.32$). Here, the streamwise component shows how a dome-like structure encloses the region in between the obstacles and it further develops in the wake. This behavior is similar to that of

the time-averaged field, thus inducing a generating process of such structures. Finally, the fifth mode can be regarded as an interaction of the above-mentioned low- and high-frequency modes, which yields flow structures resulting from the combination of such modes.

To sum up, it has been shown that the turbulent flow in urban environments can be analyzed by means of different modal-decomposition algorithms. The HODMD algorithm has shown some dynamic-mode decomposition modes could be connected to the main mechanisms to generate and break the dominant structures, such as the arch or the horseshoe vortices. Therefore, the obtained temporal modes have been classified into two different groups depending on what mechanisms they contain, the vortex-generator modes or the vortex-breaker modes.

The former appear in the low-frequency region of the spectrum (e.g., $\omega_m = 0.11$) and they generate the vortical structures through three different flow features: the dome in the streamwise direction, the cap in the wall-normal direction, and two columns in the spanwise direction. Meanwhile, the latter appear in the high-frequency portion of the spectrum (e.g., $\omega_m = 1.1$) and break the main structures creating the turbulent wake via three large size structures: the high-velocity clusters on the sides of the buildings in the streamwise direction, other high-velocity clusters that appear between the buildings for the wall-normal velocity and, finally, the arrowhead-like structures that appear between the buildings in the spanwise direction.

As mentioned above, the coherent structures delay the dispersion of the pollutant; thus, it could be interesting to reduce the appearance and energy of the A modes and enhance the B modes. Also, the most unfavorable structures present in the generator modes appear to be the streamwise dome and the wall-normal cap, since they might contribute in the concentration of the pollutants in the city. On the other hand, regarding the breaker-modes, the most favorable flow features (regarding the pollutant concentration) can be related to the spanwise arrowhead-like structures that might help the flow with the pollutants to escape from the urban region. Finally, the tunnel-shaped vortex, which is created when the arch vortex is broken, could help to redirect the pollutants retained between the buildings to the atmosphere by creating a recirculation area between the positive and negative values

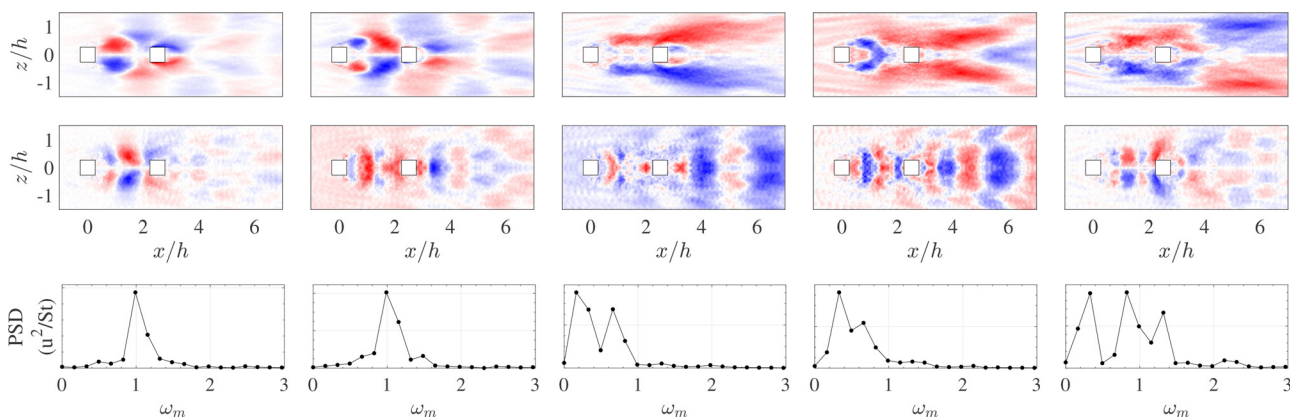


FIG. 5. (From left to right) First five POD modes at $y/h = 0.25$ (where h is the obstacle height) for the WI case, where we show (top) the streamwise and (middle) spanwise components. Contours are normalized with the L_∞ -norm and range between -1 (blue) and $+1$ (red). (Bottom) Power-spectral density scaled with the Strouhal number $St = fL/U_\infty$ of the temporal coefficients from the POD modes, where f is the characteristic frequency of each mode, $L = h$ is the characteristic length, and U_∞ is the freestream velocity.

of the structures in the B modes. Further studies should be carried out in this line using multi-phase flows, connecting the aforementioned flow structures with the particle dispersion mechanisms.

R.V. acknowledges the financial support of the Göran Gustafsson foundation. A.M.S. and S.H. were funded by Contract No. RTI2018-102256-B-I00 of Ministerio de Ciencia, innovación y Universidades/FEDER. A.C. and S.L.C. acknowledge Grant No. PID2020-114173RB-I00 funded by MCIN/AEI/10.13039/501100011033. The computations carried out in this study were made possible by resources provided by the Swedish National Infrastructure for Computing (SNIC).

AUTHOR DECLARATIONS

Conflict of Interest

The authors have no conflicts to disclose.

DATA AVAILABILITY

The data that support the findings of this study are available from the corresponding author upon reasonable request.

REFERENCES

- ¹European Commission, *Urbanisation Worldwide* (European Commission, 2018).
- ²G. Manoli, S. Fatichi, M. Schlöpfer, K. Yu, T. W. Crowther, N. Meili, P. Burlando, G. G. Katul, and E. Bou-Zeid, "Magnitude of urban heat islands largely explained by climate and population," *Nature* **573**, 55–60 (2019).
- ³R. Vinuesa, H. Azizpour, I. Leite, M. Balaam, V. Dignum, S. Domisch, A. Felländer, S. D. Langhans, M. Tegmark, and F. Fuso Nerini, "The role of artificial intelligence in achieving the Sustainable Development Goals," *Nat. Commun.* **11**, 233 (2020). [arXiv:1905.00501](https://arxiv.org/abs/1905.00501).
- ⁴S. Becker, H. Lienhart, and F. Durst, "Flow around three-dimensional obstacles in boundary layers," *J. Wind Eng. Ind. Aerodyn.* **90**, 265–279 (2002).
- ⁵H. Kawai, Y. Okuda, and M. Ohashi, "Near wake structure behind a 3D square prism with the aspect ratio of 2.7 in a shallow boundary layer flow," *J. Wind Eng. Ind. Aerodyn.* **104–106**, 196–202 (2012).
- ⁶R. J. Martinuzzi and B. Havel, "Interfering surface-mounted cubic obstacles in tandem," *J. Fluids Eng.* **122**, 24–31 (2000).
- ⁷R. J. Martinuzzi and M. AbuOmar, *Study of the Flow around Surface-Mounted Pyramids* (Springer-Verlag, 2003).
- ⁸M. AbuOmar and R. J. Martinuzzi, "Vortical structures around a surface-mounted pyramid in a thin boundary layer," *J. Wind Eng. Ind. Aerodyn.* **96**, 769–778 (2008).
- ⁹B. Monnier, S. A. Goudarzi, R. Vinuesa, and C. Wark, "Turbulent structure of a simplified urban fluid flow studied through stereoscopic particle image velocimetry," *Boundary-Layer Meteorol.* **166**, 239–268 (2018).
- ¹⁰R. Vinuesa, P. Schlatter, J. Malm, C. Mavriplis, and D. S. Henningson, "Direct numerical simulation of the flow around a wall-mounted square cylinder under various inflow conditions," *J. Turbul.* **16**, 555–587 (2015).
- ¹¹B. M. Sumer, N. Christiansen, and J. Fredsøe, "The horseshoe vortex and vortex shedding around a vertical wall-mounted cylinder exposed to waves," *J. Fluid Mech.* **332**, 41–70 (1997).
- ¹²Á. Martínez-Sánchez, E. Lazpita, A. Corrochano, S. L. Clainche, S. Hoyas, and R. Vinuesa, "Data-driven assessment of arch vortices in urban flows," [arXiv:2202.01667](https://arxiv.org/abs/2202.01667) (2021).
- ¹³P. Torres, S. Le Clainche, and R. Vinuesa, "On the experimental, numerical and data-driven methods to study urban flows," *Energies* **14**, 1310–1338 (2021).
- ¹⁴T. R. Oke, "Street design and urban canopy layer climate," *Energy Build.* **11**, 103–113 (1988).
- ¹⁵J. L. Lumley, "The structure of inhomogeneous turbulent flows," in *Atmospheric Turbulence and Radio Wave Propagation* (Nauka, 1967).
- ¹⁶J. M. Vega and S. Le Clainche, *Higher Order Dynamic Mode Decomposition and Its Applications* (Elsevier, 2020).
- ¹⁷H. Y. Zhu, C. Y. Wang, H. P. Wang, and J. J. Wang, "Tomographic PIV investigation on 3D wake structures for flow over a wall-mounted short cylinder," *J. Fluid Mech.* **831**, 743–778 (2017).
- ¹⁸J. W. Cooley and J. W. Tukey, "An algorithm for the machine calculation of complex Fourier series," *Math. Comput.* **19**, 297–301 (1965).
- ¹⁹C. Mendez, S. Le Clainche, R. Moreno-Ramos, and J. M. Vega, "A new automatic, very efficient method for the analysis of flight flutter testing data," *Aerosp. Sci. Technol.* **114**, 106749 (2021).